Received: 24 January 2020 | Revised: 19 August 2020 | Accepted: 21 August 2020

DOI: 10.1002/nbm.4409

RESEARCH ARTICLE

NMR IN BIOMEDICINE WILEY

Fully self-gated free-running 3D Cartesian cardiac CINE with isotropic whole-heart coverage in less than 2 min

Thomas Küstner[1] | Aurelien Bustin[1] | Olivier Jaubert[1] | Reza Hajhosseiny[1] | Pier Giorgio Masci[1] | Radhouene Neji[1,2] | René Botnar[1,3] | Claudia Prieto[1,3]

[1]School of Biomedical Engineering and Imaging Sciences, King's College London, St. Thomas' Hospital, London, UK

[2]MR Research Collaborations, Siemens Healthcare Limited, Frimley, UK

[3]Escuela de Ingeniería, Pontificia Universidad Católica de Chile, Santiago, Chile

Correspondence
Thomas Küstner, School of Biomedical Engineering and Imaging Sciences, King's College London, St. Thomas' Hospital, Lambeth Wing, London, UK.
Email: thomas.kuestner@kcl.ac.uk

Funding information
Engineering and Physical Sciences Research Council, Grant/Award Numbers: EP/P001009/1, EP/P007619/1, EP/P032311/1; Wellcome Trust, Grant/Award Number: NS/A000049/1

Purpose: To develop a novel fast water-selective free-breathing 3D Cartesian cardiac CINE scan with full self-navigation and isotropic whole-heart (WH) coverage.

Methods: A free-breathing 3D Cartesian cardiac CINE scan with a water-selective balanced steady-state free precession and a continuous (non-ECG-gated) variable-density Cartesian sampling with spiral profile ordering, out-inward sampling and acquisition-adaptive alternating tiny golden and golden angle increment between spiral arms is proposed. Data is retrospectively binned based on respiratory and cardiac self-navigation signals. A translational respiratory-motion-corrected and cardiac-motion-resolved image is reconstructed with a multi-bin patch-based low-rank reconstruction (MB-PROST) within about 15 min. A respiratory-motion-resolved approach is also investigated. The proposed 3D Cartesian cardiac CINE is acquired in sagittal orientation in 1 min 50 s for 1.9 mm^3 isotropic WH coverage. Left ventricular (LV) function parameters and image quality derived from a blinded reading of the proposed 3D CINE framework are compared against conventional multi-slice 2D CINE imaging in 10 healthy subjects and 10 patients with suspected cardiovascular disease.

Results: The proposed framework provides free-breathing 3D cardiac CINE images with 1.9 mm^3 spatial and about 45 ms temporal resolution in a short acquisition time (<2 min). LV function parameters derived from 3D CINE were in good agreement with 2D CINE (10 healthy subjects and 10 patients). Bias and confidence intervals were obtained for end-systolic volume, end-diastolic volume and ejection fraction of 0.1 ± 3.5 mL, −0.6 ± 8.2 mL and −0.1 ± 2.2%, respectively.

Conclusion: The proposed framework enables isotropic 3D Cartesian cardiac CINE under free breathing for fast assessment of cardiac anatomy and function.

Abbreviations: ADMM, alternating direction method of multipliers; bSSFP, balanced steady-state free precession; CS, compressed sensing; EDV, end-diastolic volume; EF, ejection fraction; ESV, end-systolic volume; FISS, fast interrupted steady state; FOV, field of view; LV, left ventricular; MB-PROST, multi-bin patch-based low-rank reconstruction; SAR, specific absorption rate; T_A, time of acquisition; WH, whole heart.

René Botnar and Claudia Prieto: these authors contributed equally.

KEYWORDS
3D CINE, bSSFP, cardiovascular imaging, Cartesian, free running, low-rank reconstruction, whole heart

1 | INTRODUCTION

Cardiac CINE MRI is the gold standard for the assessment of cardiac morphology and function.[1,2] In clinical routine, multi-slice 2D CINE is performed under multiple breath-holds to achieve left ventricular (LV) coverage. This requires patient cooperation and can result in slice misalignments due to different or imperfect breath-hold positions. 2D free-breathing CINE imaging with retrospective respiratory motion correction[3–7] and single breath-hold 2D real-time acquisitions[8] have been proposed to minimize slice misalignment and improve patient comfort. In order to provide functional information for, eg, wall motion insufficiency, reformats into arbitrary orientations are required. The above approaches achieved only anisotropic resolution, for which high-resolution reformats to arbitrary orientations are not feasible. Thus, multiple acquisitions in several geometric views are required, which increases overall planning and scan time. In order to counter these limitations, ideally images with isotropic resolution should be acquired.

Motion-corrected super-resolution frameworks have been proposed to enhance through-plane resolution of 2D CINE by reconstructing pseudo-3D cardiac CINE datasets from multiple multi-slice anisotropic 2D volumes.[9–11] However, this requires long acquisitions (and complex planning) of several low-resolution volumes (∼10 min), and their performance heavily depends on the accuracy of slice-to-slice/volume registrations.

Accelerated acquisitions with parallel imaging and compressed sensing (CS) reconstruction[12–16] have been proposed to enable single breath-hold 3D cardiac CINE (∼10 to 27 s). However, due to the limited breath-hold duration these techniques needed to make tradeoffs between temporal resolution, LV coverage and anisotropic slice resolution (2.5 to 10 mm).

To address the above limitations, free-breathing 3D CINE,[17–28] so called free-running methods, with non-Cartesian (spiral phyllotaxis,[19,24] radial stack of stars,[25–27,29] 3D radial koosh-ball[17,18,22,30]) or Cartesian trajectories (MUSIC,[28] centric reordering,[23] CASPR[21]), have been proposed to provide isotropic resolution with whole-heart (WH) coverage. Non-Cartesian approaches have shown promising image quality in scan times of about 10-15 min for high spatial isotropic resolutions (∼1.05 to 1.5mm^3) or shorter scan times of about 5-8 min for anisotropic resolutions (1-2 mm in plane, 3-8 mm through plane). For Cartesian sampling, scan times of about 4-8 min for about 2 mm^3 isotropic resolution have been achieved. For sufficient contrast, some methods apply an interruption with T_2 preparation pulses[17,19,24] or rely on the administration of contrast agents.[18,21–23,25,28] In free-breathing CINE, fat-related artifacts can arise from high signal intensities of the subcutaneous fat that becomes aliased within the field of view (FOV) due to motion and undersampling. Fat suppression techniques such as interleaved spectral selective fat saturation pulses,[19,24] multi-echo balanced steady-state free precession (bSSFP),[27] fast interrupted steady state (FISS)[31–33] or lipid insensitive binomial off-resonance excitation (LIBRE)[34] have been proposed to counteract these.

In the reconstruction, data is usually binned into cardiac and respiratory phases based on ECG,[17–24,26–28] self-gated cardiac[25,35] or respiratory[17–27,35] signals. Motion-resolved/corrected images are then reconstructed exploiting temporal redundancy in both cardiac and respiratory directions, using primarily regularized CS-based reconstructions.[17,21,23,25,26,28] Non-Cartesian trajectories usually require long reconstruction times, of the order of hours, associated with regridding operations at each iteration of the reconstruction.

In this work, we propose a 3D Cartesian free-running cardiac CINE to acquire isotropic WH coverage in a clinically feasible scan time of less than 2 min (spatial resolution 1.9 mm^3) and about 15 min reconstruction time. A non-contrast-enhanced, water-selective 3D bSSFP sequence is proposed. A previously proposed variable-density spiral-like Cartesian trajectory (VD-CASPR)[36] is extended in this work to continuous CINE sampling. In order to fully exploit spatio-temporal redundancies with an intrinsic motion alignment amongst patches of different temporal phases, we have recently proposed multi-bin patch-based low-rank reconstruction (MB-PROST)[20,37] which is 3D patch-based low-rank reconstruction[38] that exploits local (within a patch), non-local (between similar patches in a neighborhood) and multi-bin (between different motion states) redundancies. In the reconstruction, cardiac-motion-resolved and respiratory-motion-corrected/resolved images are obtained from retrospective binning via cardiac and respiratory self-navigation signals followed by a soft-weighted MB-PROST reconstruction. The proposed method was evaluated in 10 healthy subjects and 10 patients with suspected cardiovascular disease in comparison with clinical gold standard multi-slice and multi-breath-hold 2D CINE imaging.

2 | METHODS

The proposed 3D free-running framework consists of: a water-selective 3D bSSFP (slab-selective) sequence with VD-CASPR sampling for free-running CINE acquisition (Figure 1) in concert with fully self-gated binning with soft-weighted MB-PROST reconstruction

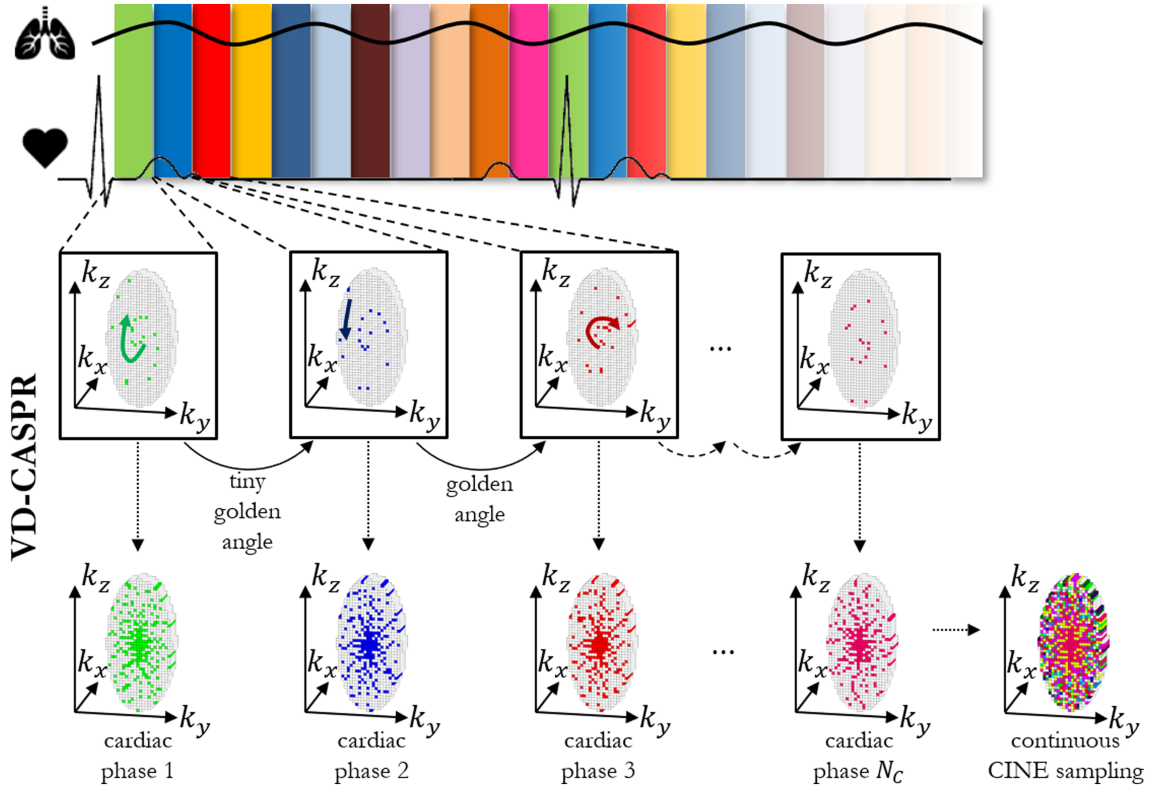

FIGURE 1 Free-running (free-breathing, non-ECG-gated) 3D CINE variable-density Cartesian acquisition with spiral profile ordering (VD-CASPR) sampling. A continuous acquisition with out-inward sampling and acquisition-adaptive alternating tiny golden and golden angle increment throughout the cardiac cycle ensures incoherent aliasing within and between cardiac phases with minimal influence of eddy currents. The tiny golden angle is derived from the number of acquired spiral arms to ensure non-redundant and incoherent sampling within and between motion states. The *k*-space center line is repeatedly acquired (once per pair of spiral arms), serving as a fully self-navigational signal. After the desired acquisition time T_A (bottom row), N_C pre-assumed cardiac phases are sampled with a prescribed acceleration factor L

(Figures 2 and 3 later) to provide 3D cardiac-motion-resolved and respiratory-motion-corrected/resolved images with WH coverage and isotropic resolution in less than 2 min.

2.1 | Acquisition

The overall temporal course of the acquisition under free-breathing is depicted in Figure 1. The VD-CASPR trajectory for 3D cardiac CINE subsamples the phase-encoding plane k_y-k_z of size $N_y \times N_z$, where N_y is the matrix size along k_y and N_z is the matrix size along k_z, in an elliptical scanning region with $N < N_y N_z$ sampling points. The trajectory samples on the Cartesian grid along a spiral-like arm with variable-density spreading. An alternating angle increment between spiral arms and out-inward sampling are applied. During the planning prior to the acquisition, based on the repetition time T_R and the desired temporal resolution for each cardiac phase (under the assumption of N_C cardiac phases), the number of sampling points R along each spiral arm is set to fully span the entire cardiac cycle RR $\approx RT_R N_C$ (normal cardiac cycle without arrythmia). In order to meet the desired acquisition time T_A the undersampling factor L is set to fulfill

$$L \simeq \frac{N \cdot \mathrm{RR}}{R \cdot T_A}. \tag{1}$$

For the non-triggered free-running acquisition, this choice of L and R showed good conditioning of the undersampling factor per cardiac and respiratory phase in a retrospective binning with an arbitrary number of cardiac and respiratory phases.

In order to evenly distribute the spiral arms in the entire cardiac cycle whilst providing (i) incoherent and non-redundant sampling between and within cardiac and respiratory phases (determined by retrospective gating) and (ii) minimal gradient switching for high-frequency samples (ie expected to minimize eddy currents), an alternating angle increment with out-inward sampling is employed. For odd numbered spiral interleaves a golden angle increment to the previous spiral arm and an outward sampling are used, whereas for even numbered spiral interleaves a

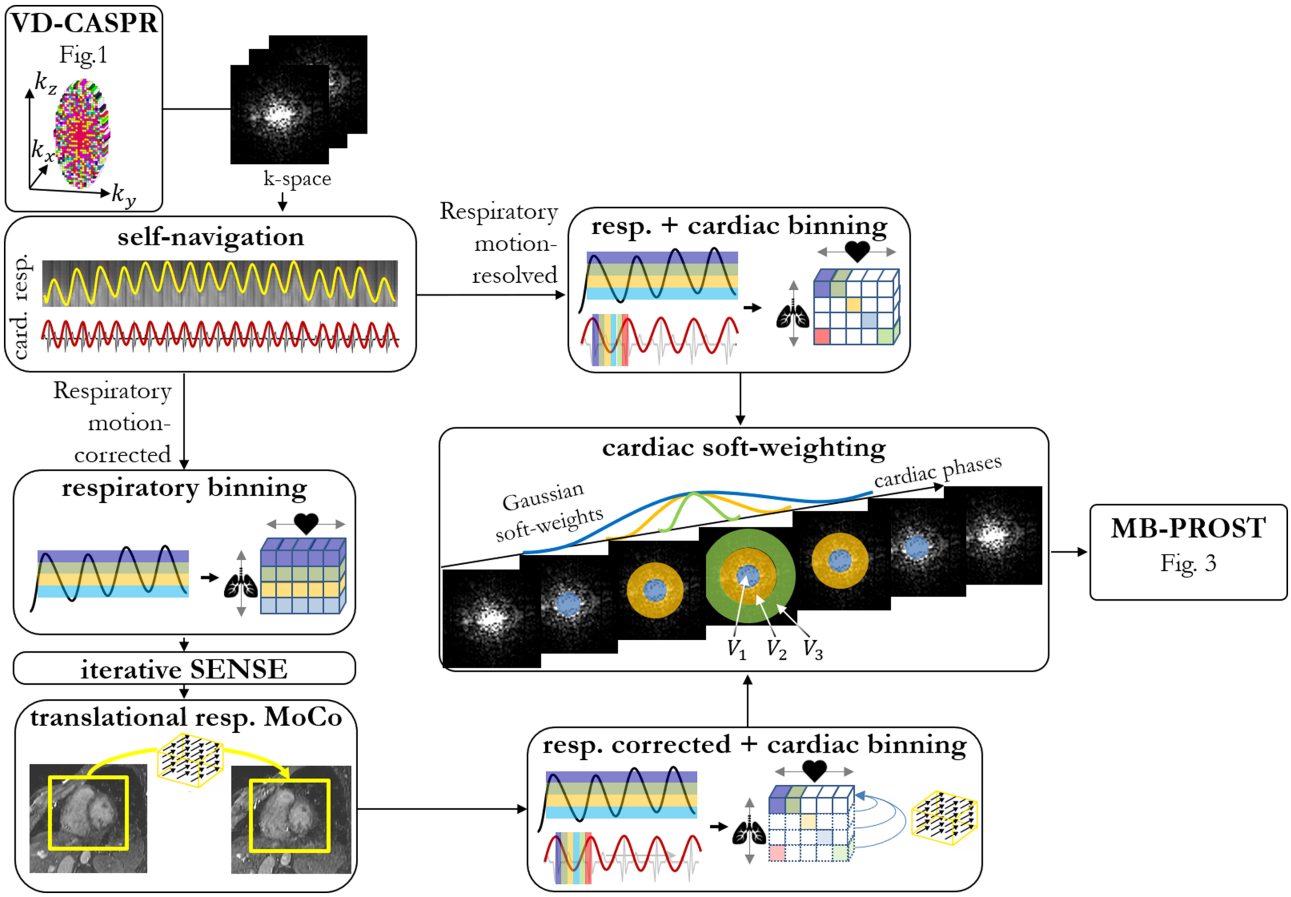

FIGURE 2 Proposed reconstruction framework to derive cardiac-motion-resolved and respiratory-motion-corrected/resolved 3D images. An automatic coil-selected and bandpass-filtered principal component analysis provides the respiratory and cardiac self-navigation signals. For the respiratory-motion-corrected approach a respiratory binning followed by an iterative SENSE reconstruction provides an auxiliary respiratory-resolved image from which 3D respiratory translational motion can be estimated. For the respiratory-motion-resolved image a simultaneous cardiac and respiratory binning is performed. Binning is performed with respiratory Gaussian soft weighting and a cardiac spatial-temporal Gaussian soft weighting between neighboring cardiac phases (here, $K = 3, V_1 = 2, V_2 = 1, V_3 = 0.5$)

sequence-adaptive tiny golden angle increment to the previous spiral arm and an inward sampling are used. The tiny golden angle of order M (Reference 39) is calculated for the total number of acquired spiral arms SP so that $SP \in G^M$ is a member of the generalized Fibonacci sequence G^M, ensuring good spatial sampling coverage and uniform filling of motion states after binning. For every second spiral arm, the k-space center line is acquired with a temporal resolution of $2RT_R$, serving as a respiratory and cardiac self-navigation signal.

2.2 | Reconstruction

An overview of the reconstruction steps is depicted in Figure 2. The respiratory and cardiac self-navigation signals are extracted via a principal component analysis of the bandpass-filtered and coil-selected k-space center lines.[18] An automatic coil selection based on energy thresholding[40] in the respiratory (2-12 s, 0.08-0.5 Hz) and cardiac (40-100 bpm, 0.66-1.66 Hz) frequency ranges guides the extraction to the relevant coils picking up the respiratory and cardiac motion. Subsequently the acquired data is binned into the respective motion states using the self-navigation signals.

Two processing modes are possible: (a) sequential respiratory and cardiac binning yielding a respiratory-motion-corrected and cardiac-motion-resolved image or (b) joint respiratory and cardiac binning yielding a respiratory and cardiac-motion-resolved image. The latter approach is more computationally demanding due to the additional respiratory motion direction.

For both modes, in the respiratory direction an amplitude-based binning with equally spaced gates between end-expiratory (95th percentile of respiratory self-navigation signal) and end-inspiratory (5th percentile) states is applied. N_R respiratory gates with neighboring view-sharing and Gaussian soft weighting are used. N_C cardiac gates linearly span the RR interval for all cardiac cycles. Cardiac cycles with arrythmias are rejected in the binning if the RR interval deviates by ±40% from the mean RR duration. To enhance sampling density a spatial-temporal cardiac soft

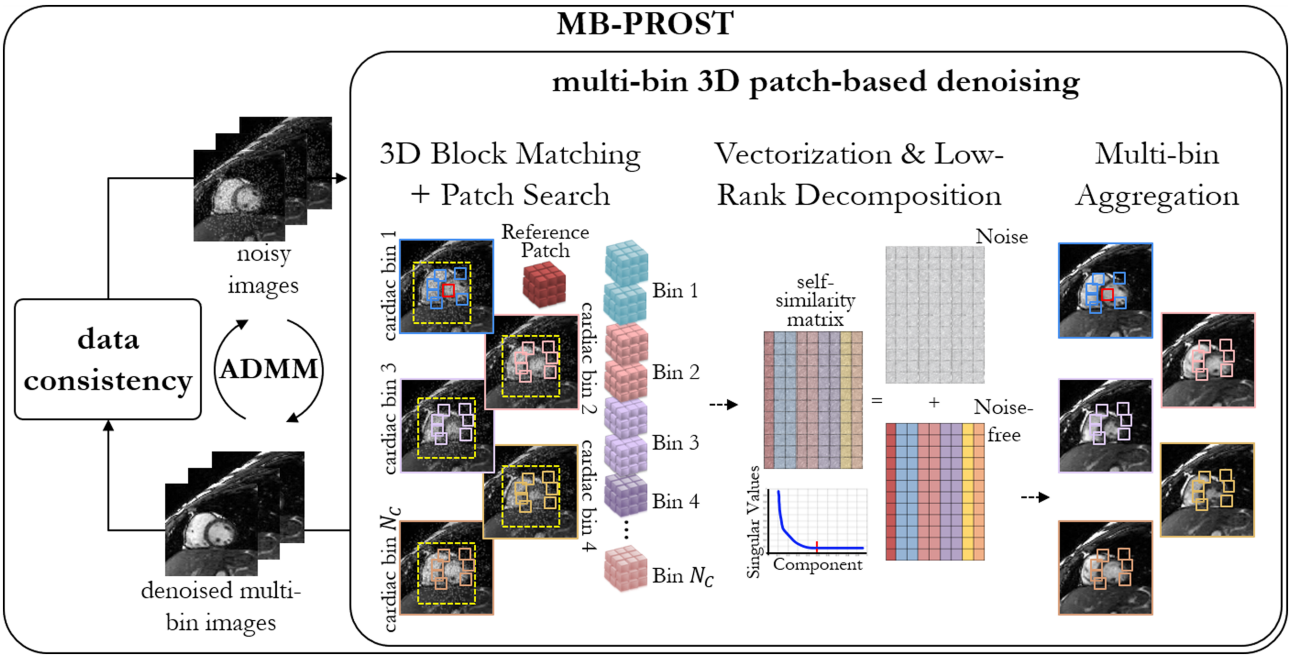

FIGURE 3 MB-PROST is solved through operator-splitting via ADMM by iteratively alternating the minimization between (i) an L2 norm data consistency for the multiple cardiac phases and (ii) a low-rank patch-based matrix denoising followed by (iii) an update of the augmented multiplier. In the multi-bin 3D patch-based denoising, patches similar to a reference patch are identified within a search window extending through all cardiac phases (dashed yellow rectangle) to form a self-similarity matrix on which a singular value decomposition is conducted. These denoised patches are aggregated back to the multi-bin image. MB-PROST reconstruction considers the soft weights (Figure 2) and a multi-coil sensitivity map derived from the fully sampled low-frequency region

weighting between neighboring cardiac gates is applied, under the assumption that homogeneous regions, ie low-frequency components, vary slowly.[41] For this, the sampling region in the k_y-k_z plane is divided into K concentric areas with varying radius $r_k, k \in [1,K]$. Each area is assigned a different view-sharing factor $V_k \in \left[0, \frac{N_C}{2}\right]$ indicating how far in the temporal direction neighboring cardiac gates can contribute samples to the current cardiac gate, as illustrated in Figure 2. For each position k_y/k_z, the soft weights are given by a Gaussian function centered at the current cardiac gate with standard deviation given by V_k. Spatially coinciding view-sharing samples are averaged.

For the respiratory-motion-resolved case, the cardiac and respiratory binning is done simultaneously with N_R respiratory and N_C cardiac states utilizing the described respiratory and cardiac Gaussian soft weighting W.

In the case of respiratory motion correction, after an initial respiratory binning (and $N_C = 1$ cardiac phase), an auxiliary respiratory-motion-resolved image is reconstructed with iterative SENSE[42] in order to estimate the translational respiratory motion (superior-inferior, left-right and anterior-posterior rigid displacement) of the heart. 3D translational respiratory motion correction towards end-expiration is performed using an optical-flow based image registration (projection of non-rigid motion fields estimated with local all pass[43]). Respiratory-motion-corrected data is subsequently binned to N_C cardiac states considering a cardiac Gaussian soft weighting W as described before.

Coil sensitivity maps $S \in \mathbb{C}^{N_x N_y N_z Ch}$ are obtained via ESPIRiT[44] from the time-averaged (across all respiratory and cardiac states) central fully sampled k-space data, where N_x, N_y, N_z represent the number of voxels in the spatial directions x,y,z and Ch is the number of MR receiver channels.

From the binned and subsampled k-space $Y \in \mathbb{C}^{N_x N_y N_z N_R N_C Ch}$, we seek to reconstruct the 5D complex image $X \in \mathbb{C}^{N_x N_y N_z N_R N_C}$ for all cardiac and respiratory motion states. For the respiratory-motion-corrected approach $N_R = 1$ after the last binning step. The respiratory-motion-resolved reconstruction is performed sequentially with MB-PROST for each of the N_R motion states.

MB-PROST assumes that 3D free-running imaging contains a rich amount of redundancy on local (intensities within a patch), non-local (between patches within a spatial neighborhood) and temporal (between cardiac phases) scales. This information can be exploited through patch-based matrix representation and singular value decomposition to regularize the overall MR reconstruction problem, yielding

$$\arg\min_{X,\mathcal{T}} \frac{1}{2}\|AWFSX - Y\|_F^2 + \lambda_P \sum_P \|\mathcal{T}_P\|_*, \text{s.t.} \mathcal{T}_P = P_P(X) \tag{2}$$

where A describes the subsampling operator, W the Gaussian soft weights, F the Fourier transform, S denotes the coil sensitivity maps, $\|\cdot\|_F$ is the Frobenius norm, $\lambda_P > 0$ is the sparsity-promoting regularization parameter for patch P and $\|\cdot\|_*$ is the nuclear norm enforcing low rank on a multi-bin patch scale. The patch selector $P_P(\cdot)$ extracts 3D patches similar to a reference patch centered at voxel P, within a given spatial-temporal

search window, amongst all cardiac phases or bins. Assuming that similar structures exist in different cardiac phases, but at different spatial locations, a search for similar patches within a search window (dashed box in Figure 3) enables exploiting temporal cardiac redundancies with implicit motion-aligned content. Similar patches are then vectorized and concatenated to form a low-rank 2D matrix $\mathcal{T}_P$ for denoising. This step is repeated for each pixel in a sliding-window fashion. Equation 2 is solved using alternating direction method of multipliers (ADMM) iteration. The principal schematics of MB-PROST are depicted in Figure 3.

2.3 | Implementation details

Reconstruction parameters were empirically optimized on several datasets (not reported here) and were maintained for all datasets. Images are binned into N_R = 8 respiratory and N_C = 16 cardiac gates (if not stated otherwise), with 25% respiratory view-sharing and cardiac spatio-temporal view-sharing factors of V_1 = 2,V_2 = 1.5,V_3 = 1.25,V_4 = 1. For MB-PROST, the degree of redundant structural information within each patch is controlled by the size of the patches and was set to 5^3 voxels. Similar 3D patches were searched in a 3D+N_c window of size $60^3 \times N_c$. 20 similar patches were selected within this spatial-temporal search window. The regularization parameter λ_P was set to 0.3. A fixed number of 3 ADMM iterations and 10 conjugate gradient iterations were performed. MB-PROST reconstruction was implemented in MATLAB (v9.6, MathWorks, Natick, MA) with the multi-bin 3D patch-based denoising implemented in C (MEX) and distributed over 12 CPUs (2.3 GHz Intel Xeon E5-2697) to provide fast computational times.

2.4 | In vivo study

Imaging was performed on a 1.5 T MRI (MAGNETOM Aera, Siemens Healthcare, Erlangen, Germany) equipped with 18-channel body and 32-channel spine coils. Written informed consent was obtained from all subjects and the study was approved by the local ethics committee.

The proposed free-running 3D Cartesian CINE was acquired with a water-selective (1-2-1 binomial pulse) bSSFP sequence in sagittal orientation. 10 healthy subjects (5 female, age = 31 ± 3 years) and 10 patients with suspected cardiovascular disease (4 female, 45 ± 21 years) with isotropic WH coverage of 1.9 mm^3 resolution were acquired under free-breathing in time of acquisition (T_A) = 1 min 50 s. The FOV was adapted to the subject's heart size providing WH coverage. Remaining imaging parameters included T_E = 2.33 ms, T_R = 4.66 ms, flip angle α = 39°, bandwidth = 1042 Hz/px, phase oversampling = 10%, slice oversampling = 15% and acceleration L = 6. To obtain N_C = 16 cardiac phases during acquisition, the number of segments per spiral arm R = 8-11 was adapted to fit within the subject's cardiac cycle (57-101 bpm, 81 ± 13 bpm). The obtained cardiac temporal resolution for N_C = 16 was 37-51 ms (45 ± 5 ms) with a temporal resolution of the self-navigation signal of 75-103 ms (90 ± 12 ms).

To investigate the influence of fat suppression, we performed in five healthy subjects (body mass indices = 18/19/22/24/26 kg/m^2) (i) a non-fat-suppressed bSSFP with T_E = 1.3 ms, T_R = 2.6 ms, α = 39°, bandwidth = 1042 Hz/px, T_A = 1 min 10 s; (ii) a FISS with n = 2 bSSFP readouts per FISS module,[32] T_E = 1.6 ms, T_{RbSSFP} = 3.2 ms, T_{RFISS} = 12.1 ms, α = 40°, bandwidth = 1230 Hz/px, T_A = 2 min 22 s, and (iii) the proposed water-selective bSSFP (parameters as stated above). All acquisitions used the same 3D Cartesian protocol described above.

To investigated the feasibility of achieving higher spatial resolution, the proposed 3D Cartesian approach was performed in seven healthy subjects (4 female, age = 32 ± 3 years) with isotropic WH coverage of 1.4 mm^3 under free breathing in T_A = 2 min 40 s. Imaging parameters included T_E = 2.44 ms, T_R = 4.84 ms and L = 8. Remaining imaging parameters were the same as the 1.9 mm^3 protocol.

A multi-slice and multi-breath-hold conventional 2D bSSFP CINE acquisition with retrospective gating and 2× GRAPPA acceleration was performed for all subjects. Non-fat suppressed 2D CINE was acquired in eight breath-holds of 12 s duration (two slices per breath-hold) each with 20 s pause in between breath-holds for recovery and instructions, resulting in an acquisition time of 3 min 56 s. 2D CINE acquisition parameters included resolution of 1.9 × 1.9 mm^2 in plane, slice thickness 8 mm, temporal resolution ∼40 ms, 20 cardiac phases (reconstructed), T_E = 1.06 ms, T_R = 2.12 ms, α = 52°, bandwidth = 915 Hz/px and LV coverage in short-axis orientation.

2.5 | Evaluation

The proposed free-running 3D Cartesian CINE is evaluated for respiratory-motion-corrected and motion-resolved reconstructions and qualitatively compared against conventional 2D CINE.

Quantitative assessment was conducted for end-systolic volume (ESV), end-diastolic volume (EDV) and ejection fraction (EF) LV function parameters in 17 healthy subjects (10 healthy subjects with 1.9 mm^3 resolution and 7 healthy subjects with 1.4 mm^3 resolution) and 10 patients (1.9 mm^3 resolution). LV epicardial and endocardial segmentation masks of free-running 3D CINE (1.4 mm^3 and 1.9 mm^3, respiratory motion corrected) and conventional 2D CINE acquisitions were automatically determined with the Segment software[45] and afterwards manually

corrected by two experienced readers (2 and 14 years of experience in cardiac MRI) when needed. Intra-reader (repeated LV measurements) and inter-reader reproducibility was assessed.

A blinded quality reading between proposed free-running 3D Cartesian CINE and conventional multi-breath-hold 2D CINE was conducted by the same two experienced readers. Readers were blinded to the acquisition strategy and were only presented with cardiac-motion-resolved images at randomly chosen slices in short-axis orientation of either 2D CINE or 3D CINE. Images were taken from both 2D CINE and 3D CINE at similar anatomical slice locations. Readers were therefore presented with the same number of 2D CINE and 3D CINE images in a randomly permutated order, ie no side-by-side scoring and no sequential scoring of 2D CINE followed by 3D CINE. FOV was cropped tightly around the heart. Readers rated the images on a five-point Likert scale (1, non-diagnostic; 2, borderline diagnostic; 3, acceptable; 4, good; 5, excellent) with respect to signal-to-noise ratio (SNR), contrast, sharpness, residual artifacts (aliasing, noise and blurring), diagnostic confidence and overall image impression, independently. A score greater than 3 is indicative of diagnostic image quality. Inter-reader agreement was assessed by Cohen's kappa.[46]

Contrast between myocardium and blood pool is measured by the contrast ratio

$$\mathrm{CR} = \frac{\mathrm{mean}(\mathrm{ROI}_{\mathrm{myocardium}})}{\mathrm{mean}(\mathrm{ROI}_{\mathrm{blood}})} \tag{3}$$

with blood pool regions of interest drawn in left and right ventricular blood pools for 2D CINE and proposed free-running 3D CINE.

Statistical significances for CR and intra-/inter-reader reproducibility were determined with a paired Welch's t-test (significance level of $P < 0.05$) and Bonferroni correction under the null hypothesis of equal means for unequal variances.

3 | RESULTS

End-systolic and end-diastolic cardiac phases of the proposed free-running 3D Cartesian water-selective CINE (1.9 mm^3) in two representative healthy subjects for sagittal (native) and reformats in coronal, short-axis, vertical long-axis (two-chamber) and horizontal long-axis (four-chamber) orientations are shown in Figure 4. Images are translational respiratory motion corrected to end-expiratory state. For comparison the conventional 2D CINE in the native short-axis is shown as well. Cardiac-motion-resolved images for these two subjects are depicted in Video A1 (Supporting Information).

Comparisons of the proposed free-running 3D CINE (respiratory motion corrected) in short-axis orientation for acquired resolution of 1.9 mm^3 (T_A = 1 min 50 s) in three healthy subjects are shown in Figure 5. In comparison to the multi-breath-hold 2D CINE images (T_A = 3 min 56 s), good visual agreement can be achieved. Cardiac-motion-resolved images are depicted in Video A2 (Supporting Information).

In Figure 6, end-systolic and end-diastolic images in short-axis orientation of the proposed free-running 3D CINE (respiratory motion corrected) in comparison to multi-breath-hold 2D CINE are depicted in three patients. The patients shown illustrate the spectrum of challenges encountered in the clinic: Patient A had arterial fibrillation, Patient B had a normal heart rate of about 65 bpm and Patient C had a high heart rate of about 90 bpm. Cardiac-motion-resolved images are depicted in Video A3 (Supporting Information).

The influence of the respiratory motion correction is investigated for healthy subjects with mild (Subject F) and strong (Subject G) breathing in Supplemental Figure A4 (Supporting Information). A comparison between the respiratory-motion-corrected (to end-expiratory state), motion-resolved (end-expiratory state) and no respiratory motion correction (ie ignoring respiratory binning) reconstruction of the proposed free-running 3D CINE for different isotropic resolutions (1.4 mm^3 and 1.9 mm^3) is shown. End-systolic and end-diastolic images are depicted. Reconstruction time was about 15 min for the respiratory-motion-corrected approach and about 90 min for the respiratory-motion-resolved approach.

A comparison for different spatial resolutions of the proposed free-running 3D CINE (respiratory motion corrected) is shown in Supplemental Figure A5 (Supporting Information) in three healthy subjects for resolutions of 1.4 mm^3 (T_A = 2 min 40 s) and 1.9 mm^3 (T_A = 1 min 50 s) in contrast to conventional multi-breath-hold 2D CINE ($1.9 \times 1.9 \times 8$ mm^3).

Varying temporal resolutions are investigated in Figure 7. The proposed sampling and the retrospective binning enable us to flexibly reconstruct almost any desired number of respiratory and cardiac states. End-systolic and end-diastolic images of two healthy subjects with varying number of cardiac phases (N_C = 16,24,32) are shown in Figure 7. The temporal evolution (temporal profiles) of cardiac phases is shown in the horizontal long-axis orientation for the left and right ventricles. Cardiac-motion-resolved images are depicted in Video A6 (Supporting Information).

Spatial LV coverage of the proposed free-running 3D CINE (respiratory motion corrected) is illustrated in comparison to conventional 2D CINE in Video A7 (Supporting Information). Not all basal slices for 3D CINE are shown.

Minimal possible T_R for the selected water-selective RF pulse and maximal flip angle under specific absorption rate (SAR) consideration were set. An average SAR of 1.9 W/kg was observed (derived from DICOMs and calculated in vendor reconstruction on scanner).

The impact of fat-related aliasing is depicted in Supplemental Figure A8 (Supporting Information) for non-fat-suppressed bSSFP, FISS with n = 2 bSSFP readouts per FISS module and the proposed water-selective bSSFP in one healthy subject with slightly elevated body mass index of

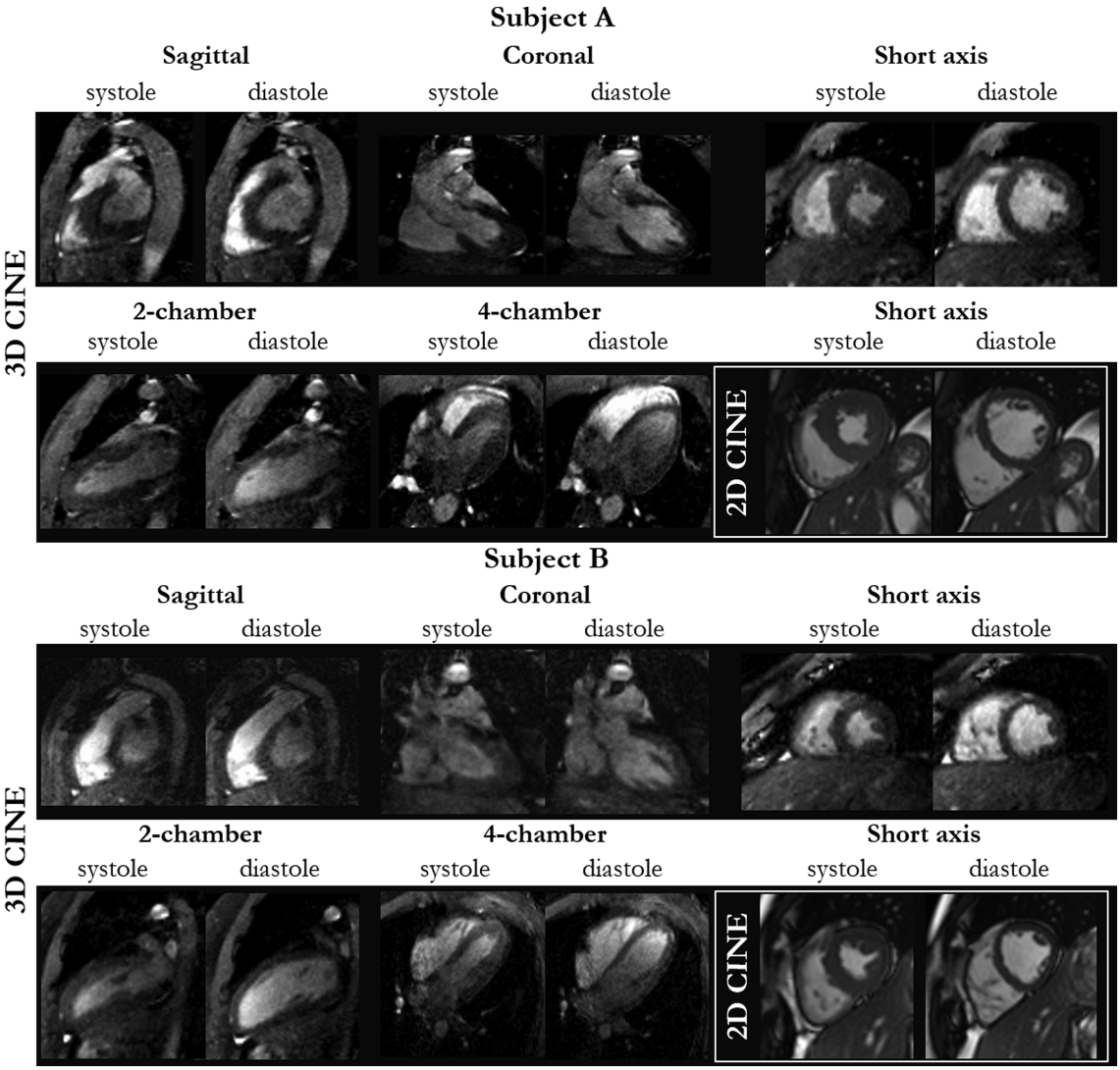

FIGURE 4 End-systolic and end-diastolic respiratory-motion-corrected images of two healthy subjects of proposed 3D Cartesian free-running CINE in sagittal (native), coronal, two-chamber, four-chamber and short-axis orientations for water-selective bSSFP sequence with 3D isotropic resolution (1.9 mm^3) WH coverage in T_A = 1 min 50 s. Comparative multi-breath-hold 2D CINE images in short-axis (non-fat-suppressed, 1.9 × 1.9 × 8 mm^3 resolution, T_A = 3 min 56 s) are depicted. Cardiac-motion-resolved images are shown in Supplemental Video A1

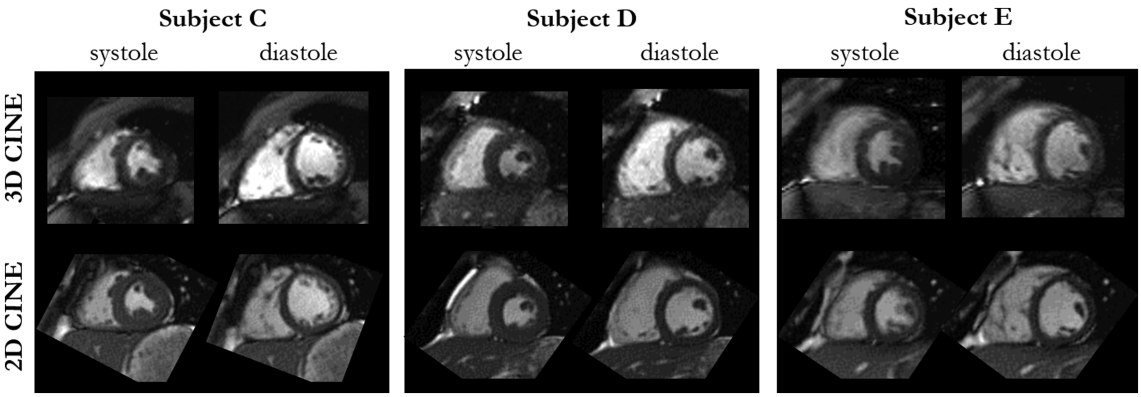

FIGURE 5 End-systolic and end-diastolic phases of respiratory-motion-corrected images acquired with proposed free-running 3D Cartesian cardiac CINE for spatial resolutions of 1.9 mm^3 (T_A = 1 min 50 s) in comparison with multi-slice multi-breath-hold 2D CINE with 1.9 × 1.9 × 8 mm^3 resolution (T_A = 3 min 56 s) in three healthy subjects. Cardiac-motion-resolved images are shown in Supplemental Video A2

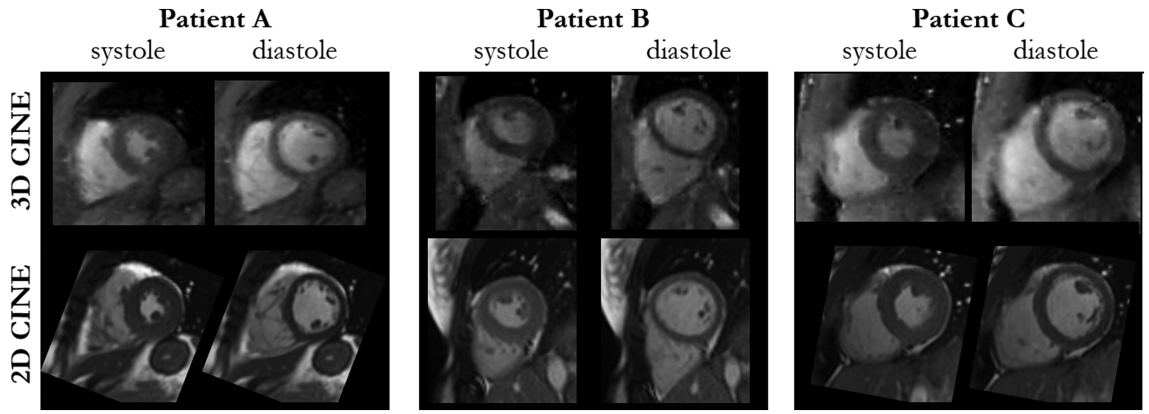

FIGURE 6 End-systolic and end-diastolic phases of proposed free-running 3D CINE (1.9 mm^3 resolution, TA = 1 min 50 s, respiratory-motion-corrected) in comparison to multi-breath-hold 2D CINE (1.9 × 1.9 × 8 mm resolution, TA = 3 min 56 s) in three patients. Patient A had arterial fibrillation, patient B had a normal heart rate ~65 bpm and patient C had a high heart rate of ~90 bpm. Cardiac-motion-resolved images are depicted in Supplemental Video A3

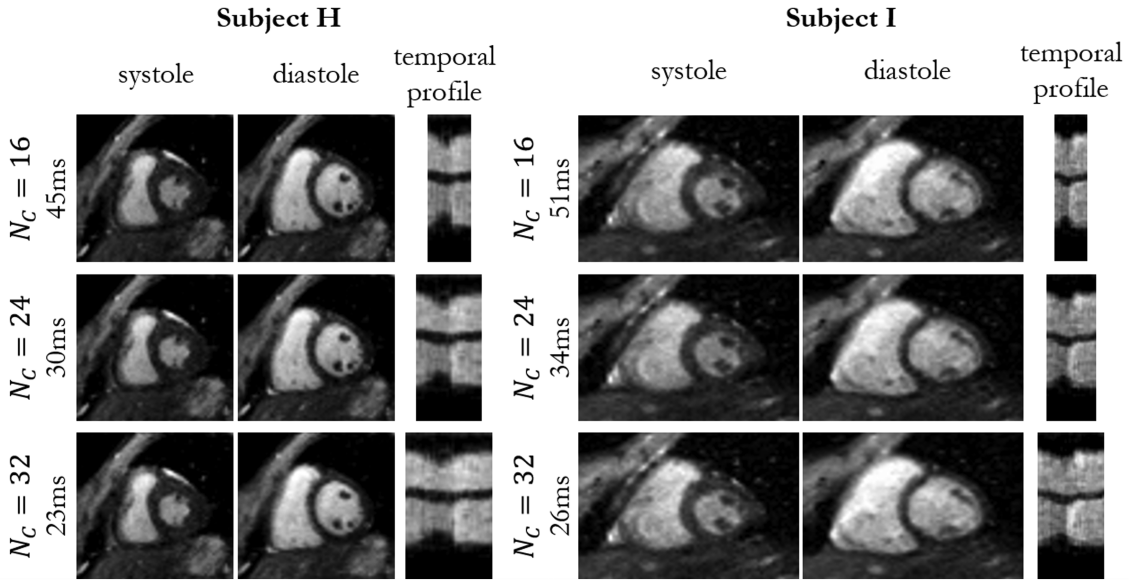

FIGURE 7 End-systolic and end-diastolic phases of respiratory-motion-corrected images in two healthy subjects for different cardiac temporal resolutions depending on the number of retrospectively binned cardiac phases and subject's heart rate. Temporal profiles indicate good depiction of cardiac function. Cardiac-motion-resolved images are shown in Supplemental Video A6

26 kg/m^2. The same number of samples were acquired with the proposed 3D CINE sampling, resulting in different acquisition times based on RF pulse duration and ramp-up/down RF pulses with gradient spoiling (FISS). Aliasing of fat content in non-fat-suppressed bSSFP can be appreciated as indicated by the arrows. FISS and water-selective bSSFP minimize fat-related aliasing. The proposed water-selective bSSFP has a shorter acquisition time than FISS, because FISS requires frequent ramp-up/down pulses and gradient spoiling. A quantitative contrast ratio analysis for five healthy subjects is shown in Supplemental Figure A9 (Supporting Information), indicating an improved contrast of about 82%/about 73% in water-selective free-running/FISS 3D CINE compared with non-fat-suppressed 3D CINE with statistically significant difference ($p < 0.001$ with $\alpha = 0.05$). No statistically significant difference between 2D CINE and the fat-suppressed 3D CINE (proposed water-selective and FISS) was observed.

The Bland-Altman plots of LV function parameters in Figure 8 (10 healthy subjects 1.9 mm^3, 10 patients 1.9 mm^3) and Supplemental Figure A10 (Supporting Information; 7 healthy subjects 1.4 mm^3) reveal high agreement between free-running 3D CINE (all respiratory motion

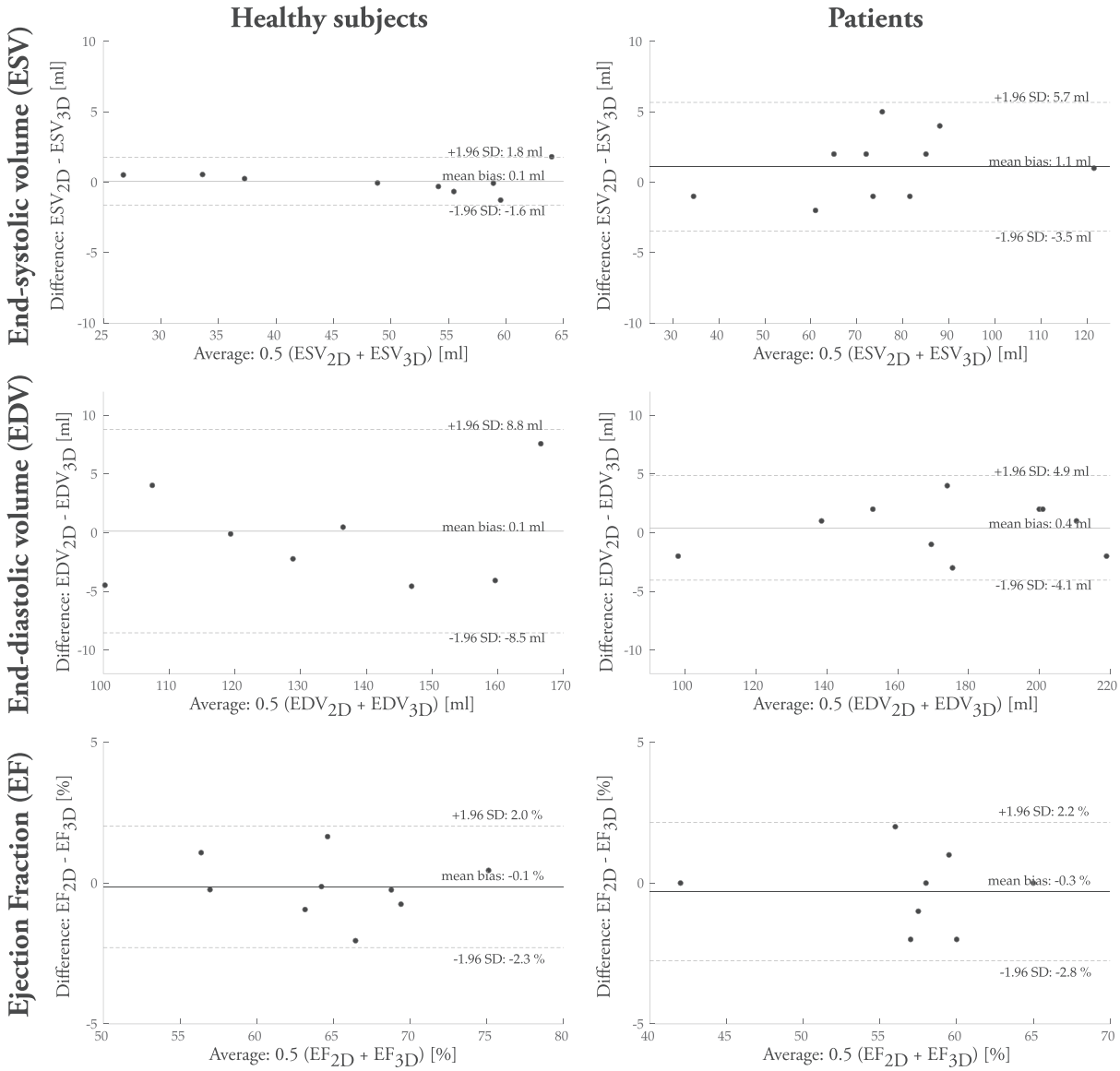

FIGURE 8 Extracted LV function parameters, ESV, EDV and EF, for proposed free-running 3D CINE (10 healthy subjects and 10 patients with 1.9 mm^3 resolution in T_A = 1 min 50 s, all respiratory motion corrected) in comparison with conventional 2D CINE. Bias and confidence intervals are stated in the results

corrected) and conventional multi-breath-hold 2D CINE. The respective scatter plots with the linear regression are shown in Supplemental Figure A10 (Supporting Information; healthy subjects with 1.4 mm^3) and Supplemental Figure A11 (Supporting Information; healthy subjects and patients with 1.9 mm^3). On average, in the healthy subjects a bias of −1.2 mL/−2.9 mL/0.2% for 1.4 mm^3 and of 0.1 mL /0.1 mL/−0.1% for 1.9 mm^3 was observed, with all observations lying inside the confidence interval of ±1.7 mL/±10.8 mL/±2.1% for 1.4 mm^3 and ±1.6 mL/±8.2 mL/±2.1% for 1.9 mm^3 in ESV/EDV/EF of the proposed 3D CINE. The values for the joint healthy subject cohort (1.4 mm^3 and 1.9 mm^3) are reported in Figure 8. In the patients, a bias of 1.1 mL/0.4 mL/−0.3% with confidence intervals of ±4.6 mL/ ±4.5 mL/ ±2.5% were observed for ESV/EDV/EF. Intra-reader and inter-reader reproducibility both showed no statistically significant difference, p = 0.69 (α = 0.05), between repeated measurements and readers. Inter-reader reproducibility was further assessed by the intra-class correlation coefficient of 0.97 ± 0.02, indicating excellent agreement.

The blinded reading revealed an overall image quality on the five-point Likert scale of 4.5 ± 0.6 for 2D CINE and 3.6 ± 0.7 for 3D CINE. Further quality scores in 2D CINE/3D CINE yielded a score of 4.2 ± 0.7/ 3.6 ± 0.7 for SNR, 4.0 ± 0.6/ 3.5 ± 0.7 for contrast, 4.2 ± 0.9/ 3.3 ± 0.8 for sharpness, 4.0 ± 0.8/3.3 ± 0.8 for residual aliasing and 4.5 ± 0.6/3.7 ± 0.6 for diagnostic confidence. In all quality scores, 3D CINE showed a scale greater than 3, indicating diagnostic usability. Inter-reader reproducibility was assessed by Cohen's kappa of 0.84, reflecting substantial agreement.

4 | DISCUSSION

An isotropic free-running (non ECG-gated, free-breathing) 3D Cartesian cardiac CINE with a water-selective bSSFP sequence is proposed with a scan time of 1 min 50 s for 1.9 mm^3 resolution. The sampling pattern with out-inward trajectory and alternating angle increment enables incoherent and non-redundant sampling between and within respiratory and cardiac motion states. Repeatedly acquired *k*-space center lines enable a fully self-gated binning in the reconstruction step. In the binning, a Gaussian soft weighting amongst neighboring motion states guarantees good conditioning for the reconstruction. A translational respiratory-motion-corrected and a respiratory-motion-resolved approach were investigated with an MB-PROST reconstruction to provide high-spatial- and temporal-resolution images.

Respiratory-motion-corrected reconstruction is carried out in about 15 min while motion-resolved reconstruction requires about 90 min (not parallelized amongst respiratory states; depending on number of respiratory states). For the motion-resolved reconstruction, one could extend MB-PROST to simultaneously exploit the respiratory and cardiac dimensions, which would however demand more computational resources. Thus, redundant temporal information could be better incorporated. Furthermore, reconstructions could be carried out on GPUs to further boost the performance. No immediate benefit of a respiratory-motion-resolved reconstruction over a motion-corrected one was observed for the proposed acquisition. On the other hand, if the respiratory motion is not handled, blurring of the heart is observed, especially in the papillary muscles and myocardium. The implicit motion alignment of patches over all cardiac phases with MB-PROST, together with soft weighting, sufficiently exploits spatial and temporal redundant information. Our experiments suggest that translational respiratory motion correction is sufficient to deal with respiration in a computationally efficient way. Retrospective binning enables us to select the desired temporal resolution improving motion depiction, which was examined for the cardiac direction but can also be used for respiration.

Good agreement between free-running 3D Cartesian CINE and conventional 2D CINE was observed in the short-axis view. In general, contrast differences between non-fat-suppressed 2D CINE and water-selective 3D CINE are expected, because of slice-selective and non-spectral-selective RF excitation in 2D CINE versus slab-selective and spectral-selective excitation in 3D CINE. Myocardium-to-blood-pool contrast can be reduced in 3D CINE due to the saturated LV blood pool and the inflow of saturated blood into the atrial pool. Furthermore, the maximum achievable flip angle in 3D CINE is lower due to SAR limitations and the T_R is increased due to water-selective RF pulses. Overall, the contrast differences were not found to be significant. The obtained results from the blinded reading in the cardiac-motion-resolved images suggest diagnostic usable quality of 3D CINE. The largest deficit of 3D CINE to 2D CINE in quality scores is observed for sharpness and residual aliasing, which might indicate residual blurring and/or aliasing along temporal direction. In future studies, tradeoffs between spatio-temporal resolution and image acceleration will be investigated to improve on these scores.

The isotropic resolution of the proposed approach enables high-resolution reformats into arbitrary orientations. Results reported in Supplemental Figure A5 and A10 suggest that a higher-resolution scan (1.4 mm^3) should be feasible with a slightly increased scan time of 2 min 40 s. Imaging with 1.9 mm^3 resolution can provide a fast assessment of cardiac function and anatomy of large vessels/cavities, and should enable investigation of wall motion or valve function.

Adipose tissue and epicardial fat can introduce strong aliasing in highly accelerated free-breathing 3D cardiac CINE. A water-selective bSSFP mitigates fat-related motion aliasing and consequently improves reconstruction quality. Binning with the cardiac self-navigator signal showed good agreement with an additionally acquired ECG signal. Myocardium-to-blood-pool contrast was sufficient for reliable extraction of ventricular functions from the free-breathing 3D CINE with high agreement with conventional multi-breath-hold 2D CINE.

The proposed sampling with suggested parametrization performed during planning together with soft-weighted view-sharing showed uniform filling per motion state after binning, even in cases with arrhythmias. Isotropic acquisition in sagittal orientation enables retrospective reformatting into arbitrary views, with planning time being greatly reduced. For the respiratory self-navigation, the readout direction should be aligned in the superior-inferior direction. Sagittal orientation was employed in this study to minimize the number of slices covering the heart while providing simplified planning; however, coronal, short-axis and vertical and horizontal long-axis orientations were also successfully tested (not reported here). Acquisition under free-breathing improves patient comfort over multiple breath-holds.

This work has some limitations. The retrospective binning always assumes an underlying cyclic motion. Any aperiodic movements can thus not be captured or resolved. In this work, we relied on water-selective RF pulses to suppress fat. The binomial pulses result in a high SAR for maximal flip angle (for good myocardium-to-blood-pool contrast), which can induce tissue warming. Although none of the scanned subjects and patients reported any negative experience or unpleasant tissue heating during the scan, investigation of other fat suppression techniques may be of interest. Given the induced RF energy and noise of the continuous free-running acquisition as well as possible changing breathing patterns, scan time should be kept short. Initial experiences with longer scan times did not reveal any marked improvement. Investigations of optimal scan time/image resolution for LV function and wall motion assessment need to be performed in future studies. Furthermore, the proposed method needs to be further validated clinically in a larger cohort to assess the clinical value with further improvements in the computational reconstruction time by, eg, GPU-based acceleration to enable a clinical feasible workflow.

5 | CONCLUSION

In this work, we present a free-running non-contrast-enhanced water-selective 3D bSSFP Cartesian cardiac CINE acquisition with 1.9 mm^3 isotropic resolution in less than 2 min scan time and about 15 min reconstruction time. Fully self-gated respiratory-motion-corrected and cardiac-motion-resolved images provide high-spatial/temporal-resolution WH coverage and show good agreement with conventional 2D CINE in healthy subjects and patients with suspected cardiovascular disease. LV functional assessment of the proposed free-running 3D Cartesian cardiac CINE shows no bias and close agreement with conventional 2D CINE.

ACKNOWLEDGEMENTS

This work was supported by the following grants: (1) EPSRC EP/P032311/1, EP/P001009/1 and EP/P007619/1; (2) Wellcome EPSRC Centre for Medical Engineering (NS/A000049/1) and (3) the Department of Health via the National Institute for Health Research (NIHR) Cardiovascular Health Technology Cooperative (HTC) and comprehensive Biomedical Research Centre awarded to Guy's & St Thomas' NHS Foundation Trust in partnership with King's College London and King's College Hospital NHS Foundation Trust. The views expressed are those of the authors and not necessarily those of the NIHR or the Department of Health and Social Care.

ORCID

Thomas Küstner https://orcid.org/0000-0002-0353-4898

REFERENCES

1. Kramer CM, Barkhausen J, Flamm SD, Kim RJ, Nagel E. Standardized cardiovascular magnetic resonance (CMR) protocols 2013 update. *J Cardiovasc Magn Reson*. 2013;15(1):91-101.
2. Puntmann VO, Valbuena S, Hinojar R, et al. Society for Cardiovascular Magnetic Resonance (SCMR) expert consensus for CMR imaging endpoints in clinical research: part I—analytical validation and clinical qualification. *J Cardiovasc Magn Reson*. 2018;20(1):67-90.
3. Schmidt M, Ekinci O, Liu J, et al. Novel highly accelerated real-time CINE-MRI featuring compressed sensing with k-t regularization in comparison to TSENSE segmented and real-time Cine imaging. *J Cardiovasc Magn Reson*. 2013;15(1):36.
4. Hansen MS, Sorensen TS, Arai AE, Kellman P. Retrospective reconstruction of high temporal resolution cine images from real-time MRI using iterative motion correction. *Magn Reson Med*. 2012;68(3):741-750.
5. Usman M, Atkinson D, Odille F, et al. Motion corrected compressed sensing for free-breathing dynamic cardiac MRI. *Magn Reson Med*. 2013;70(2):504-516.
6. Larson AC, Kellman P, Arai A, et al. Preliminary investigation of respiratory self-gating for free-breathing segmented cine MRI. *Magn Reson Med*. 2005;53(1):159-168.
7. Xue H, Kellman P, Larocca G, Arai AE, Hansen MS. High spatial and temporal resolution retrospective cine cardiovascular magnetic resonance from shortened free breathing real-time acquisitions. *J Cardiovasc Magn Reson*. 2013;15(1):102-102.
8. Vincenti G, Monney P, Chaptinel J, et al. Compressed sensing single-breath-hold CMR for fast quantification of LV function, volumes, and mass. *JACC Cardiovasc Imaging*. 2014;7(9):882-892.
9. Bhatia KK, Price AN, Shi W, Hajnal JV, Rueckert D. Super-resolution reconstruction of cardiac MRI using coupled dictionary learning. In: *2014 IEEE 11th International Symposium on Biomed Imaging (ISBI)*. New York City: IEEE; 2014:947-950.
10. Oktay O, Bai W, Lee M, et al. Multi-input cardiac image super-resolution using convolutional neural networks. In: Ourselin S, Joskowicz L, Sabuncu M, Unal G, Wells W, eds. *Medical Image Computing and Computer-Assisted Intervention—MICCAI 2016*. Cham, Switzerland: Springer; 2016:246-254.
11. Odille F, Bustin A, Liu S, et al. Isotropic 3D cardiac cine MRI allows efficient sparse segmentation strategies based on 3D surface reconstruction. *Magn Reson Med*. 2018;79(5):2665-2675.
12. Kressler B, Spincemaille P, Nguyen TD, et al. Three-dimensional cine imaging using variable-density spiral trajectories and SSFP with application to coronary artery angiography. *Magn Reson Med*. 2007;58(3):535-543.
13. Wetzl J, Schmidt M, Pontana F, et al. Single-breath-hold 3-D CINE imaging of the left ventricle using Cartesian sampling. *Magn Reson Mater Phys Biol Med*. 2018;31(1):19-31.
14. Barkauskas KJ, Rajiah P, Ashwath R, et al. Quantification of left ventricular functional parameter values using 3D spiral bSSFP and through-time non-Cartesian GRAPPA. *J Cardiovasc Magn Reson*. 2014;16(1):65-78.
15. Wech T, Pickl W, Tran-Gia J, et al. Whole-heart cine MRI in a single breath-hold—a compressed sensing accelerated 3D acquisition technique for assessment of cardiac function. *RoFo*. 2014;186(1):37-41.
16. Makowski MR, Wiethoff AJ, Jansen CH, et al. Single breath-hold assessment of cardiac function using an accelerated 3D single breath-hold acquisition technique—comparison of an intravascular and extravascular contrast agent. *J Cardiovasc Magn Reson*. 2012;14(1):53-61.
17. Feng L, Coppo S, Piccini D, et al. 5D whole-heart sparse MRI. *Magn Reson Med*. 2018;79(2):826-838.
18. Pang J, Sharif B, Fan Z, et al. ECG and navigator-free four-dimensional whole-heart coronary MRA for simultaneous visualization of cardiac anatomy and function. *Magn Reson Med*. 2014;72(5):1208-1217.
19. Coppo S, Piccini D, Bonanno G, et al. Free-running 4D whole-heart self-navigated golden angle MRI: initial results. *Magn Reson Med*. 2015;74(5):1306-1316.
20. Küstner T, Bustin A, Cruz G, et al. 3D Cartesian free-running cardiac and respiratory resolved whole-heart MRI. *Proc Int Soc Magn Reson Med*. 2019;1:2192.
21. Usman M, Ruijsink B, Nazir MS, Cruz G, Prieto C. Free breathing whole-heart 3D CINE MRI with self-gated Cartesian trajectory. *Magn Reson Imaging*. 2017;38:129-137.

22. Qi H, Jaubert O, Bustin A, et al. Free-running 3D whole heart myocardial T_1 mapping with isotropic spatial resolution. *Magn Reson Med*. 2019;82(4):1331-1342.
23. Moghari MH, Barthur A, Amaral ME, Geva T, Powell AJ. Free-breathing whole-heart 3D cine magnetic resonance imaging with prospective respiratory motion compensation. *Magn Reson Med*. 2018;80(1):181-189.
24. Piccini D, Littmann A, Nielles-Vallespin S, Zenge MO. Spiral phyllotaxis: the natural way to construct a 3D radial trajectory in MRI. *Magn Reson Med*. 2011;66(4):1049-1056.
25. Liu J, Spincemaille P, Codella NC, Nguyen TD, Prince MR, Wang Y. Respiratory and cardiac self-gated free-breathing cardiac CINE imaging with multi-echo 3D hybrid radial SSFP acquisition. *Magn Reson Med*. 2010;63(5):1230-1237.
26. Spincemaille P, Liu J, Nguyen T, Prince MR, Wang Y. Z intensity-weighted position self-respiratory gating method for free-breathing 3D cardiac CINE imaging. *Magn Reson Imaging*. 2011;29(6):861-868.
27. Liu J, Nguyen TD, Zhu Y, et al. Self-gated free-breathing 3D coronary CINE imaging with simultaneous water and fat visualization. *PLoS ONE*. 2014;9(2):1-8, e89315.
28. Han F, Rapacchi S, Khan SN, et al. 4-dimensional, multiphase, steady-state imaging with contrast enhancement (MUSIC) in the heart; a feasibility study in children. *J Cardiovasc Magn Reson*. 2015;17(1):Q131–134.
29. Park J, Larson AC, Zhang Q, Simonetti O, Li D. 4D radial coronary artery imaging within a single breath-hold: cine angiography with phase-sensitive fat suppression (CAPS). *Magn Reson Med*. 2005;54(4):833-840.
30. Chan RW, Ramsay EA, Cunningham CH, Plewes DB. Temporal stability of adaptive 3D radial MRI using multidimensional golden means. *Magn Reson Med*. 2009;61(2):354-363.
31. Bastiaansen JAM, Piccini D, Di Sopra L, et al. Natively fat-suppressed 5D whole-heart MRI with a radial free-running fast-interrupted steady-state (FISS) sequence at 1.5T and 3T. *Magn Reson Med*. 2020;83(1):45-55.
32. Küstner T, Bustin A, Jaubert O, Neji R, Prieto C, Botnar R. 3D Cartesian fast interrupted steady-state (FISS) imaging. *Magn Reson Med*. 2019;82(5):1617-1630.
33. Koktzoglou I, Edelman RR. Radial fast interrupted steady-state (FISS) magnetic resonance imaging. *Magn Reson Med*. 2018;79(4):2077-2086.
34. Bastiaansen JAM, van Heeswijk RB, Stuber M, Piccini D. Noncontrast free-breathing respiratory self-navigated coronary artery cardiovascular magnetic resonance angiography at 3T using lipid insensitive binomial off-resonant excitation (LIBRE). *J Cardiovasc Magn Reson*. 2019;21(1):38-49.
35. Di Sopra L, Piccini D, Coppo S, Stuber M, Yerly J. An automated approach to fully self-gated free-running cardiac and respiratory motion-resolved 5D whole-heart MRI. *Magn Reson Med*. 2019;82(6):2118-2132.
36. Prieto C, Doneva M, Usman M, et al. Highly efficient respiratory motion compensated free-breathing coronary MRA using golden-step Cartesian acquisition. *J Magn Reson Imaging*. 2015;41(3):738-746.
37. Küstner T, Bustin A, Neji R, Botnar R, Prieto C. 3D Cartesian whole-heart CINE MRI exploiting patch-based spatial and temporal redundancies. In: *Proceedings of the European Society for Magnetic Resonance in Medicine (ESMRMB)*. Wien: Springer Nature; 2019.
38. Bustin A, Ginami G, Cruz G, et al. Five-minute whole-heart coronary MRA with sub-millimeter isotropic resolution, 100% respiratory scan efficiency, and 3D-PROST reconstruction. *Magn Reson Med*. 2019;81(1):102-115.
39. Wundrak S, Paul J, Ulrici J, et al. Golden ratio sparse MRI using tiny golden angles. *Magn Reson Med*. 2016;75(6):2372-2378.
40. Küstner T, Würslin C, Schwartz M, et al. Self-navigated 4D Cartesian imaging of periodic motion in the body trunk using partial k-space compressed sensing. *Magn Reson Med*. 2017;78(2):632-644.
41. Cheng JY, Zhang T, Ruangwattanapaisarn N, et al. Free-breathing pediatric MRI with nonrigid motion correction and acceleration. *J Magn Reson Imaging*. 2015;42(2):407-420.
42. Pruessmann KP, Weiger M, Börnert P, Boesiger P. Advances in sensitivity encoding with arbitrary *k*-space trajectories. *Magn Reson Med*. 2001;46(4):638-651.
43. Gilliam C, Küstner T, Blu T. 3D motion flow estimation using local all-pass filters. In: *IEEE 13th International Symposium on Biomedical Imaging (ISBI)*. IEEE; 2016:282-285.
44. Uecker M, Lai P, Murphy MJ, et al. ESPIRiT—an eigenvalue approach to autocalibrating parallel MRI: where SENSE meets GRAPPA. *Magn Reson Med*. 2014;71(3):990-1001.
45. Heiberg E, Sjogren J, Ugander M, Carlsson M, Engblom H, Arheden H. Design and validation of Segment—freely available software for cardiovascular image analysis. *BMC Med Imaging*. 2010;10(1):1-13.
46. McHugh ML. Interrater reliability: the kappa statistic. *Biochem Med*. 2012;22(3):276-282.

SUPPORTING INFORMATION

Additional supporting information may be found online in the Supporting Information section at the end of this article.

How to cite this article: Küstner T, Bustin A, Jaubert O, et al. Fully self-gated free-running 3D Cartesian cardiac CINE with isotropic whole-heart coverage in less than 2 min. *NMR in Biomedicine*. 2021;34:e4409. https://doi.org/10.1002/nbm.4409